Effect of embedment on consolidated undrained capacity of skirted circular foundations in soft clay under planar loading

Published in Canadian Geotechnical Journal 54(2):158-172

http://dx.doi.org/10.1139/cgj-2016-0265

Cristina Vulpe (corresponding author)

Research Associate

Centre for Offshore Foundation Systems & ARC Centre of Excellence for Geotechnical Science and Engineering

University of Western Australia, Perth, WA 6009, Australia

Tel: +61 8 6488 7051 Fax: +61 8 6488 1044

Email: cristina.vulpe@uwa.edu.au

Susan M. Gourvenec

Professor

Centre for Offshore Foundation Systems & ARC Centre of Excellence for Geotechnical Science and Engineering

University of Western Australia, Perth, WA 6009, Australia

Tel: +61 8 6488 3995 Fax: +61 8 6488 1044

Email: susan.gourvenec@uwa.edu.au

Alexander F. Cornelius

Graduate Structural Engineer

Pritchard Francis, Subiaco, WA 6904, Australia (formerly a student in the School of Civil, Environmental and Mining Engineering at the University of Western Australia)

Tel: +61 8 9382 5111

Email: alex.fc@pfeng.com.au

No. of words: 4864 (excluding abstract, acknowledgements and references)

No. of tables: 10

No. of figures: 17

ABSTRACT

The effect of foundation embedment ratio and soil-skirt interface roughness on the consolidated undrained capacity of skirted circular foundations under planar loading in normally consolidated clay has been investigated through coupled three-dimensional finite element analyses. Results are presented as failure envelopes, and changes in shape and size of the normalised VHM failure envelopes are described as a function of relative magnitude and duration of applied preload. The results show that embedment ratio and interface roughness affect the load distribution within the soil mass, but that consolidated undrained capacity under planar loading scales proportionately with the (unconsolidated) undrained capacity of the foundation. This latter feature enables the results to be neatly synthesised into a relatively straightforward method for use in engineering practice for prediction of gain in undrained VHM capacity due to preload and consolidation.

Key words: skirted foundation; consolidation; combined loading; bearing capacity; soil-structure interface

INTRODUCTION

Skirted foundations are a type of shallow foundation used offshore that consists of a surface plate fitted with skirts that penetrate into the seabed confining a soil plug. Skirted foundations are used extensively offshore for supporting structures ranging from large gravity base structures (GBS) to relatively small subsea structures and have potential to support arrays of offshore wind turbines (Svano & Tjelta, 1996, Yun & Bransby, 2003, Byrne & Houlsby 2003, Jostad & Andersen, 2006, Mana et al., 2010, Vulpe et al., 2013). Skirted foundations are required to achieve embedment in an offshore environment as groundworks or burial are not usually practical.

Foundation embedment ratio, defined as the ratio of skirt depth to foundation plate diameter (d/D), and soil-skirt interface roughness, defined as a proportion of the undrained strength in the soil mass ($\alpha_{su}s_u$) affect the distribution of self-weight loading on the surrounding soil (Gourvenec & Randolph 2010). For the case of a rough soil-skirt interface, part of the foundation load is carried by skirt friction resulting in lower pressures beneath the base plate compared to the case of a smooth soil-skirt interface for which the entire foundation load is carried as base pressure. The proportion of load carried by skirt friction increases with increasing embedment ratio of rough skirted foundations. This results in lower excess pore pressure generation in the soil beneath the foundation and subsequent lower consolidation settlement and gain in undrained shear strength for the case of a rough soil-skirt interface compared with a smooth soil-skirt interface, all other things being equal. The effect of embedment ratio and soil-skirt interface roughness on the consolidation response of skirted foundations has been considered for a homogeneous elastic half space (Gourvenec & Randolph 2010), but these analyses by definition, cannot address the effect of consolidation on changes in capacity.

The effect of consolidation on the undrained vertical capacity of shallow foundations has been previously investigated (Zdravkovic et al. 2003, Lehane & Jardine 2003, Lehane & Gaudin 2005, Chatterjee et al. 2012, Gourvenec et al. 2014, Vulpe & Gourvenec 2014, Fu et al. 2015). A limited number of studies have addressed combined load capacity following consolidation for surface foundations (Bransby 2002, Vulpe et al. 2016), shallowly embedded rectangular subsea frames (Feng & Gourvenec 2015) and pipelines (Chatterjee et al. 2014). The effect of interface roughness and moderate embedment on consolidated undrained combined load response of shallow foundations has not been previously considered.

In this paper, a generalised framework method for predicting the consolidated undrained capacity of circular skirted foundations under planar loading as a function of relative magnitude and duration of preload, foundation embedment ratio and soil-skirt interface roughness is proposed. This study builds on a hardening law approach based on critical state soil mechanics presented by Gourvenec et al. (2014), which has been applied to other boundary value problems involving consolidated undrained multi-directional loading (e.g. Chatterjee et al. 2014, Feng & Gourvenec 2015, Vulpe et al. 2016).

FINITE ELEMENT MODEL

The program of 3D small-strain finite element analyses was performed using Abaqus commercial finite element computer software (Dassault Systemes, 2012).

Numerical model

3D finite element meshes of skirted circular foundations with embedment depth to foundation diameter ratios d/D = [0, 0.10, 0.25, 0.50] were modelled. A skirt thickness to foundation diameter ratio t_s/D = 0.005 for all embedment ratios was considered. The t_s/D modelled in this study is typical of steel skirted foundations in the field (e.g., Bye et al. 1995). Due to symmetry along the vertical centreline of the foundation, only half of the problem was modelled. Figure 1 illustrates a typical finite element mesh used in the analyses. The soil was represented by first-order full integration stress–pore fluid continuum elements (namely, C3D8P elements from the standard Abaqus library). The mesh boundaries extend a distance equal to 10 times the foundation diameter horizontally from the foundation edge and vertically from the mudline. The extent of the boundaries was shown to be sufficient so that no soil deformations or pore water pressure changes were observed at the constrained boundaries of the mesh and the failure mechanisms were unaffected. The boundary around the model circumference was constrained against out-of-plane displacement and the base of the mesh was constrained in all three coordinate directions. The free surface of the mesh, unoccupied by the foundation, was prescribed as a drainage boundary; the other mesh boundaries and the foundation were modelled as impermeable.

The skirted foundations were represented as rigid bodies with a single reference point (RP) located at skirt tip level along the centreline of the foundation (Figure 2) and were assumed "wished-in-place". Installation is therefore not explicitly modelled, but stress changes around the skirts due to tip bearing and skirt-soil interface shearing are captured during subsequent loading of the foundation.

The skirt internal wall-soil interface was prescribed as fully-bonded; the skirt outer wall-soil interface was prescribed as either fully-bonded (i.e., rough in shear and no separation allowed) or fully-smooth (frictionless). The skirt internal wall-soil interface was assumed fully-bonded based on centrifuge experimental evidence (Chen and Randolph, 2007) and particle image velocimetry analyses (Mana et al., 2012) where the internal soil plug remained fully attached to the skirt compartment due to suction. Gaps along the soil-skirt interface are expected to form and remain open on overconsolidated soil deposits (Britto and Kusakabe, 1982; Supachawarote et al., 2005; Mana et al., 2013). Thus, separation was not permitted under tensile normal forces since only normally consolidated soil was considered in this study.

The models were benchmarked against available theoretical solutions of ultimate limit states under pure vertical load (Martin, 2003; Martin and Randolph, 2001), horizontal load and moment (Randolph and Puzrin, 2003) for the surface foundation. The skirted foundation models could not be directly validated due to a lack of theoretical solutions. The surface foundation mesh was continuously refined in the areas critical for the multi-directional failure mechanisms to develop until no further improvement of the results was obtained. Once the surface foundation mesh was validated, the same meshing procedure was applied for the skirted foundations. This procedure resulted in FE models with between 50,000 and 75,000 elements depending on soil heterogeneity and embedment ratio.

Soil parameters

The coupled elasto-plastic pore fluid – stress behaviour investigated in the current study is described by the Modified Cam Clay (MCC) critical state model (Roscoe and Burland, 1968). The MCC parameters were obtained from element testing on kaolin clay (Stewart, 1992) and are summarized in Table 1. The implementation of MCC in Abaqus uses a Mises surface in the π-plane and associated flow was adopted for the plastic potential by defining the flow stress ratio as unity. Normally consolidated clay conditions were considered in this study as relevant to many deepwater seabeds. The in situ void ratio and in situ undrained shear strength profile of the normally consolidated clay are determined as follows.

The soil is considered to be one-dimensionally normally consolidated, with the in situ earth pressure coefficient given as

$$K_0 = 1 - \sin\phi' \tag{1}$$

where ϕ' is the critical state friction angle, determined from the model parameters λ, κ and M_{cs}. The in situ effective stresses (σ'_v and σ'_h) vary accordingly to the prescribed soil unit weight (Table 1).

The initial size of yield surface of the critical state model is defined as

$$(p'_0)^2 - p'_0 p'_c + \frac{q_0^2}{M_{cs}^2} = 0 \tag{2}$$

where p_c', p_0' and q_0 represent the preconsolidation stress, initial effective mean stress and deviatoric stresses; M_{cs} is the slope of the critical state line

$$M_{cs} = \frac{6 \sin\phi'}{3 - \sin\phi'} \tag{3}$$

The subscript ‘cs’ is used to distinguish the label from that adopted for moment, M.

The initial void ratio of a soil element is given by

$$e_0 = e_1 - \kappa p'_0 - (\lambda - \kappa) \ln p'_c \tag{4}$$

where λ represents the slope of the virgin consolidation line and critical state line and κ is the slope of the recompression line.

$$e_1 = e_\Gamma + (\lambda - \kappa) \ln 2 \tag{5}$$

with e_Γ the void ratio on the critical state line when $p' = 1$ kPa.

The relationship between the undrained shear strength of the soil, s_u, and the in situ effective vertical stress, σ'_v is given by (Potts and Zdravkovic, 1999)

$$\frac{s_u}{\sigma'_v} = g(\theta)\cos(\theta)\frac{1+2K_0}{3}\left(\frac{1+A^2}{2}\right)^{1-\frac{\kappa}{\lambda}} \tag{6}$$

where

$$g(\theta) = \frac{\sin\phi'}{\cos\theta + \frac{1}{\sqrt{3}}\sin\theta\sin\phi'} \quad 7$$

$$A = \frac{\sqrt{3}(1 - K_0)}{g(-30°)(1 + 2K_0)} \quad 8$$

with θ = -30° the Lode angle for triaxial compression conditions.

A surcharge equivalent to 1 m of soil overburden, σ'_{vo}, was imposed on the soil mass at the free surface in order to avoid zero shear strength at the mudline (s_{um}). The shear strength profile of normally consolidated clay with linearly increasing shear strength is defined by

$$s_u = s_{um} + k_{su} z \quad 9$$

where s_u represents the shear strength of the soil at depth z. For the MCC parameters and surcharge adopted in this study, the shear strength gradient k_{su} = 1.75 kPa/m and the shear strength at mudline s_{um} = 4.79 kPa. The magnitude of the unconsolidated undrained bearing capacity and relative gain in consolidated undrained capacity varies accordingly to the resulting soil heterogeneity index $\kappa_{su} = k_{su}D/s_{um}$. Nonetheless, the generalized theoretical framework presented in this study is shown to incorporate the effect of soil overburden in predicting the relative gain in consolidated undrained capacity of circular foundations (Vulpe et al. 2016).

PROGRAM OF ANALYSES

The study presented in this paper investigated the consolidated undrained response of skirted circular foundations under multi-directional loading as a function of normalised magnitude and duration of self-weight preload, embedment ratio and soil-skirt interface roughness. Over 3,500 fully coupled 3D FE analyses were performed in this program.

Initially, analyses were carried out to determine the unconsolidated undrained vertical bearing capacities (V_{uu}) for each embedment ratio d/D and soil-skirt interface condition. The soil was brought to failure in undrained conditions through displacement-control. The vertical displacement was applied to the foundation RP (i.e. concentrically at skirt tip level). Failure was defined as when a plastic plateau was observed in the load-displacement response, i.e. continued plastic strain at constant applied load.

Subsequently, analyses were performed to determine the uniaxial and multi-directional capacity for each foundation embedment ratio interface condition as a function of relative magnitude and duration of preload. In summary:

- A vertical preload (V_p) was imposed, in undrained conditions, as a fraction of the V_{uu} relative to the foundation system, taking values of V_p/V_{uu} = [0.1, 0.7] at intervals of 0.1.
- Full primary consolidation was prescribed by allowing the excess pore water pressure resulting from the applied relative preload to dissipate. Periods corresponding to 20, 30, 50 and 80% of the full primary consolidation were subsequently considered.
- The soil was brought to failure in undrained conditions by imposing displacement-controlled probe tests on the skirted foundation at the RP level. Failure was sought under uniaxial vertical (V), horizontal (H) and moment (M), and in combined VHM space. Failure under uniaxial loading was defined as when a plastic plateau was observed in load-displacement response, i.e. continued plastic strain at constant applied load. Failure under combined loading was defined by the terminating point of the associated probe test.

A list of notations for resultant loads is given in Table 2. The sign convention for this study is summarized in Figure 2 and follows the recommendations outlined by Butterfield et al (1997).

RESULTS

Excess pore water pressure generation

Excess pore water pressure is generated in the soil around a foundation upon application of a preload. Figure 3 illustrates the initial contact pressure across the base plate of a skirted foundation with embedment ratio of d/D = 0.25 for both rough and smooth soil-skirt interfaces. Contact pressure is taken as the initial increase in excess pore pressure Δu_i normalized by the applied bearing pressure v_p ($v_p = V_p/A$ where A represents the cross-sectional area of the base plate), for discrete relative preload levels V_p/V_{uu} = 0.1, 0.4 and 0.7. The initial excess pore pressure ratio increases with increasing applied relative preload irrespective of interface roughness. A smaller relative contact pressure is observed beneath the base plate for the rough-skirted foundation as part of the preload is carried by the interface friction along the skirts. In contrast, the preload is carried exclusively by the base plate and skirt tip for the smooth-skirted foundation.

The proportion of relative preload carried by base bearing is influenced by embedment ratio d/D. Figure 4 shows the initial contact pressure in a soil element located at the mudline at the centreline of the base plate. The results from the current study are plotted against the contact pressures observed beneath a surface circular foundation (Vulpe et al. 2015). Rough skirted foundations with greater embedment ratio will carry more relative preload as skirt friction through a higher surface contact area than for lower embedment ratios. As a result, the relative contact pressure decreases with increasing embedment ratio for the rough soil-skirt interface. In contrast, for a smooth soil-skirt interface, the contact pressure increases with increasing embedment ratio as the applied pressure is carried only by the base plate and skirt tips. At low embedment ratios, a portion of the applied load is shed laterally into the surrounding soil reducing the contact pressure. This lateral shedding also takes place for rough-skirted foundations but is masked by the effect of skirt friction.

Consolidation response

The time required to achieve partial or full primary consolidation is expressed through the dimensionless time factor T as

$$T = \frac{c_{v0} t}{D^2} \tag{10}$$

where c_{v0} is the initial coefficient of consolidation

$$c_{v0} = \frac{k(1 + e_0)p_0'}{\lambda \gamma_w} \tag{11}$$

with k representing the permeability and γ_w = 9.81 kN/m^3 the unit weight of water, t is the actual time passed following application of preload and D is the foundation base plate diameter. Notations T_{20}, T_{30}, T_{50}, T_{80} represent the dimensionless time required for 20, 30, 50 and 80% of the full primary consolidation to occur. Full primary consolidation is denoted by T_{99}.

Figure 5 shows the time-settlement response of a skirted circular foundation with embedment ratio d/D = 0.25 for relative preloads of V_p/V_{uu} = [0.1, 0.7] at intervals of 0.1 for both rough and smooth soil-skirt interfaces. Only the consolidation settlement w_c is shown, i.e., the initial settlement following preload application is deducted from the total settlement. The consolidation settlement increases with applied relative preload irrespective of soil-skirt interface conditions and embedment ratio. The consolidation settlement of the smooth skirted foundations is consistently higher than for the rough skirted foundations for all levels of relative preload. This arises as a result of the rough soil-skirt interface carrying a proportion of the preload by friction, resulting in lower contact pressure under the base plate and lower excess pore water pressure generated compared to the same foundation geometry and loading conditions for a smooth skirted foundation. The higher excess pore water pressure generation, due to the one-dimensional nature of consolidation within the confined soil plug, results in higher settlement.

The influence of embedment ratio on consolidation settlement is illustrated in Figure 6 for rough-skirted foundations under a range of relative preload levels. The dimensionless consolidation settlement is shown to increase with increasing embedment ratio for the same relative preload. The effect of embedment ratio on the consolidation settlement response becomes more pronounced at higher relative preloads. Although the same relative preload V_p/V_{uu} is applied, the absolute magnitude of V_p increases with increasing embedment ratio (since V_{uu} increases with increasing d/D) and a higher excess pore water pressure is generated. The consolidation settlement for all embedment ratios is similar for very low relative preload since little excess pore water is generated.

Gain in shear strength of soil following consolidation

Preloading followed by consolidation leads to an increase in soil shear strength in the vicinity of a foundation. Figure 7 shows the effect of the magnitude of relative preload and embedment ratio on the increase in undrained shear strength following full primary consolidation. The increase in undrained shear strength is illustrated through contours of enhanced in situ soil strength, $s_{u,f}/s_{u,i}$ defined by

$$\frac{s_{u,f}}{s_{u,i}} = \exp\left(\frac{e_0 - e_f}{\lambda}\right) \qquad 12$$

where $s_{u,i}$ and $s_{u,f}$ are the initial (pre-consolidation) and final (post-consolidation) shear strength, respectively, e_0 and e_f are the in situ and final void ratio, respectively, and $\lambda = 0.205$ is the virgin compression index for kaolin clay (Stewart, 1992). The greatest gain in undrained shear strength is achieved at foundation edges (for d/D = 0) and around the skirt tip (for d/D > 0) and diminishes with distance from the zone of maximum gain. Higher excess pore pressure is generated under higher relative preload levels, V_p/V_{uu}, resulting in higher relative gain in shear strength with increasing relative preload. The extent, or bulb, of excess pore pressure generation is essentially independent of the level of preload (simply scaled by depth as a function of the surface value). However, greater excess pore pressure generation translates into greater gains in strength at a given depth. The zone of gain in shear strength extends deeper with increasing embedment ratio since longer skirts carry loading deeper into the soil, but the extent of the zone of influence beneath tip level is essentially independent of d/D.

The effect of soil-skirt interface roughness on the gain in shear strength throughout the soil domain is illustrated in Figure 8 for a range of foundation embedment ratios. The gain in soil strength is concentrated beneath tip level for a smooth skirted foundation while strength increase is observed adjacent to the rough foundation skirts. As such, the magnitude of gain in shear strength inside the skirt compartment and around the skirt tip is lower compared to the same areas for the smooth skirted foundation counterpart. The extent of the bulb of relative gain in shear strength below the skirt tip is very similar for both rough and smooth soil-skirt interfaces.

Consolidated undrained uniaxial capacity

Full primary consolidation

The relative gains in vertical, horizontal and moment uniaxial capacity of circular skirted foundations after vertical preloading and full primary consolidation are shown in Figure 9 - Figure 11. The figures show relative gain in uniaxial capacity as the ratio of consolidated undrained capacity to unconsolidated undrained capacity (see Table 2 for notations). The term uniaxial is used to define loading in a singular direction following vertical preloading, for example, loading to failure in the horizontal direction concurrently with the applied relative preload (but no additional vertical or moment loading). The relative gain in capacity increases with increasing relative preload for all loading directions. The relative gain in uniaxial vertical and horizontal capacity decreases with increasing embedment ratio, but no clear trend in moment capacity can be linked to embedment ratio. The relative gain in capacity can be explained by the overlap between the zones of gain in shear strength and the governing failure mechanism in the soil mass, as illustrated in Figure 12.

The highest relative gain in capacity is associated with horizontal loading (Figure 10), followed by moment loading (Figure 11) and the lowest relative gains are associated with vertical loading (Figure 9). The failure mechanisms under uniaxial horizontal loading (Figure 12b) are the shallowest compared with other loading directions while the failure mechanisms under uniaxial vertical loading (Figure 12a) extend deepest into the soil mass, intersecting the zones of least gain in soil strength. The relative gain in horizontal capacity is greater for rough skirted foundations than for smooth skirted foundations for all levels of embedment ratio $d/D > 0$ as the failure mechanism extends laterally into the soil mass where little or no increase in shear strength is obtained for smooth skirted foundations. The relative gain in moment capacity is also greater for rough skirted foundations, but to a lesser degree as the failure mechanism extends slightly outside the skirt external wall into stronger soil. On the contrary, the relative gain in vertical capacity is marginally larger for smooth skirted foundations – the failure mechanism for smooth skirted foundations cuts through zones of higher increase in undrained shear strength during failure under vertical loading.

Critical state framework for predicting uniaxial gains

The increase in consolidated undrained uniaxial capacity can be estimated through a theoretical method based on critical state soil mechanics (Gourvenec et al. 2014). The mobilised soil is treated as a single ‘operative’ soil element, scaled to account for the non-uniform distribution of stress and strength increase across the soil domain. The operative increment in plastic stress (i.e. leading to plastic strain), $\Delta\sigma_{pl}'$, following preloading can be estimated as

$$\Delta\sigma'_{pl} = f_{\sigma} \frac{V_p}{A} \tag{13}$$

where A is the bearing area of the foundation, and f_{σ} is a factor to account for the non-uniform distribution of stress in the affected zone of soil.

The resulting increase in strength of the affected soil, i.e., the 'operative shear strength', is then calculated as

$$\Delta s_u = f_{su} R\left(\Delta\sigma'_{pl}\right) = f_{\sigma} f_{su} f_d R\left(\frac{V_p}{A}\right) \tag{14}$$

where the shear strength factor f_{su} scales the gain in strength of the 'operative' soil element to that mobilised during subsequent failure and R is the normally-consolidated strength ratio of the soil (Equation 6), which is 0.279 for the parameters given in Table 1. Separate scaling factors f_{σ} and f_{su} allow the response in over consolidated conditions to be captured, but in the present normally consolidated conditions there is effectively a single scaling parameter, $f_{\sigma}f_{su}$. The scaling factors $f_{\sigma}f_{su}$ for circular surface foundations was defined by Vulpe et al. (2016) for uniaxial vertical, horizontal and moment capacity and are summarized in Table 3**.** The scaling factor $f_{\sigma}f_{su}$ is uniquely defined for circular foundations and is independent of actual foundation size, MCC soil properties and applied soil overburden stress (Vulpe et al. 2016, Feng & Gourvenec 2015).

An additional scaling factor to account for the non-linear effect of the embedment ratio f_d is introduced in this study

$$f_d = \alpha_d \left(\frac{V_p}{V_{uu}}\right)^{\beta_d} \tag{15}$$

Changes in capacity scale with changes in operative strength, so that

$$\frac{V_{cu}}{V_{uu}}, \frac{H_{cu}}{H_{uu}}, \frac{M_{cu}}{M_{uu}} = 1 + \frac{\Delta s_u}{s_u} = 1 + f_\sigma f_{su} R \alpha_d \left(\frac{V_p}{V_{uu}} \right)^{\beta_d + 1} N_{cV} \qquad 16$$

Coefficients α_d and β_d are defined for both rough and smooth skirted circular foundations as a function of embedment ratio for each uniaxial capacity through polynomial functions.

$$\alpha_d = 1 + \alpha_{d,1}\left(\frac{d}{D}\right) + \alpha_{d,2}\left(\frac{d}{D}\right)$$

$$\beta_d = \beta_{d,1}\left(\frac{d}{D}\right) + \beta_{d,2}\left(\frac{d}{D}\right) \qquad 17$$

Values of coefficients α_d and β_d are given in Table 4.

Comparison between the finite element results and the critical state soil mechanics framework (Equation 16) - defined as ‘theoretical prediction’ in this study - shows good agreement (Figure 9, Figure 10 and Figure 11).

Figure 13a and 13b illustrate in a critical state framework the stress-volume changes of a soil element at the mudline beneath the centreline of the base plate of the surface circular foundation following preloading, consolidation and undrained failure due to uniaxial vertical loading. The results are shown in effective mean stress (p′) – deviatoric stress (q) space and effective mean stress (lnp′) – void ratio (e) space. The effective mean stress p′ represents the spherical stress responsible for volumetric deformations (compression) within the soil mass and is proportional to applied preload level and the deviatoric stress q is the stress relevant to ultimate limit state where the deviatoric stress at failure (q_f) is defined as twice the undrained shear strength of the soil s_u. The stress path representation in Figure 13 enables the coupling of the compression, evidenced by a decrease in soil void ratio, and shear response of the soil to be observed. It is evident that void ratio reduces with increasing preload leading to higher mobilizable deviatoric stress (analogous to undrained shear strength) following consolidation. Thus, the increase in undrained shear strength is proportional to the decrease in soil void ratio.

Partial consolidation

Waiting for full primary consolidation in a field situation is often impractical and as such, the maximum potential gain in capacity may not be achieved. However, partial consolidation can significantly enhance soil shear strength and hence capacity. Figure 14 illustrates the evolution of the proportion of maximum potential gain in undrained vertical and horizontal capacity as a function of consolidation time for both rough and smooth skirted circular foundations with d/D = 0.50. A simple equation linking the consolidation time, represented by the non-dimensional time factor T, and the proportion of maximum potential gain (i.e. following full primary consolidation) is proposed:

$$\frac{V_{cu,p}-V_{uu}}{V_{cu}-V_{uu}},\frac{H_{cu,p}-H_{uu}}{H_{cu}-H_{uu}},\frac{M_{cu,p}-M_{uu}}{M_{cu}-M_{uu}}=\frac{1}{1+\left(\dfrac{T}{m_i T_{50,s}}\right)^{n_i}} \qquad 18$$

with $T_{50,g}=m_i T_{50,s}$ (non-dimensional time required for 50% of the potential maximum uniaxial capacity to occur). The partial relative gains in undrained uniaxial capacity, $V_{cu,p}$, $H_{cu,p}$ and $M_{cu,p}$ may be determined from Equation (18). The non-dimensional time factor for 50% consolidation settlement, $T_{50,s}$, is given in Table 5 for each embedment ratio and soil-skirt interface roughness. The fitting coefficient m_i, where i = V, H or M, accounts for the difference between achieving 50% consolidation settlement and 50% of the potential maximum gain in capacity and is given in Table 6 for each loading direction. It results that 50% of V_{cu} is achieved 20% faster than the equivalent consolidation settlement while the gain in horizontal and moment capacity lags about 15% behind the consolidation settlement. The fitting coefficient n_i = -1.20 irrespective of foundation embedment ratio or loading type.

Equation (18) represents a conservative assessment of the potential maximum gain in uniaxial horizontal and moment capacity for rough skirted foundations. A better fit may be achieved by

$$\frac{H_{cu,p} - H_{uu}}{H_{cu} - H_{uu}}, \frac{M_{cu,p} - M_{uu}}{M_{cu} - M_{uu}} = \frac{1}{1 + \frac{V_p / V_{uu}}{0.7}\left(\frac{T}{m_i T_{50}}\right)^{n_i}} \tag{19}$$

Figure 14 indicates good agreement between the FEA results and the relative gains in undrained uniaxial capacity derived from Equations (18) and (19).

Consolidated undrained VHM capacity

Failure envelopes in horizontal and moment load space (H-M) for various levels of relative vertical preload followed by full primary consolidation are compared with the unconsolidated undrained case in Figure 15 for both rough and smooth skirted foundations with d/D = 0.5. The failure envelopes are presented in dimensionless form as $h = H/H_{uu}$ versus $m = M/M_{uu}$.

Preloading without consolidation leads to a reduction in available HM capacity (Figure 15a and b) while capacity following preloading and consolidation leads to an increase in available HM capacity (Figure 15c and d).

The results in Figure 15 also show that the shape of the normalised HM failure envelope for any given relative preload is similar for the consolidated undrained and unconsolidated undrained cases, as has been observed for other foundation geometries (Vulpe et al, 2016, Feng & Gourvenec 2015). Therefore, the consolidated undrained failure envelopes may be constructed by scaling the undrained unconsolidated failure envelope by the normalised consolidated undrained uniaxial capacities h_{cu} and m_{cu} respectively.

Approximating expression

An approximating elliptical expression describing the unconsolidated undrained failure envelope of shallow foundations can be expressed as

$$\left(\left|\frac{h}{h^*}\right|\right)^{\alpha} + \left(\frac{m}{m^*}\right)^{\alpha} + 2\beta\frac{hm}{h^*m^*} = 1 \qquad 20$$

The form of the equation was originally proposed for prediction of unconsolidated undrained capacity of shallow strip foundations under general loading (Gourvenec and Barnett, 2011). The equation was afterwards adapted for prediction of unconsolidated undrained capacity of skirted circular foundations (Vulpe et al. 2014, Vulpe, 2015).

Coefficients α and β are the fitting parameters dependent on the foundation embedment ratio, soil shear strength heterogeneity index and soil-skirt interface. Values of α and β are summarized in Table 7 for skirted circular foundations with rough soil-skirt interface and in Table 8 for skirted circular foundations with smooth soil-skirt interface. These fitting parameters are repeated here from Vulpe (2015) for convenience. The effect of vertical preloading, explicitly absent from Eqn. 20, is accounted for through the definition of the ultimate horizontal and moment capacity for the applied preload, h^* and m^*

$$h^* = 1 - \left(\frac{V_p}{V_{uu}}\right)^{4.14}$$

$$m^* = 1 - \left(\frac{V_p}{V_{uu}}\right)^{2.12} \qquad 21$$

The expressions for h^* and m^* represent the lower limits of the failure envelopes in vertical and horizontal or vertical and moment load space. Values of h_{max}/h^*, where h_{max} represents the maximum horizontal mobilization as a result of horizontal-moment loading crosscoupling, which are required to satisfactorily reproduce the shape of the failure envelopes, are given in Table 9 for the rough and smooth interfaces, respectively. Curve fits using the approximating expression (Eq. 20) scaled by the normalized consolidated undrained uniaxial horizontal and moment capacities. H_{cu}/H_{uu} and M_{cu}/M_{uu}, (Eq. 16) show good agreement with the FE results (Figure 16).

Failure envelopes for partially consolidated conditions can be determined from the failure envelope after full primary consolidation by applying horizontal and moment scaling factors $h_{cu,p}/h_{cu}$ and $m_{cu,p}/m_{cu}$, respectively. Failure envelopes for varying degrees of consolidation for a given relative preload and embedment ratio predicted by the finite element analyses are shown in Figure 17 and compared with the approximating expression showing a close fit.

A summary of the methodology to determine the partially and fully consolidated undrained capacity of rough and smooth skirted circular foundations under multi-directional loading is presented in Table 10.

CONCLUDING REMARKS

Results of small-strain finite element analyses have quantified the effect of embedment ratio and soil-skirt interface roughness on the multi-directional undrained capacity of skirted circular foundations as a function of relative magnitude and duration of self-weight preloading.

The following conclusions may be drawn from this study:

- Gain in capacity is governed by the interaction of the zone of increase in undrained shear strength of the soil and the kinematic mechanism at failure. Greatest relative gain in capacity was achieved under pure horizontal load, as the failure mechanism cuts through soil of highest gain in undrained shear strength. The lowest relative gain was achieved under pure vertical load since the failure mechanism intersects zones of lowest shear strength increase.

- The gain in undrained shear strength, and consequently capacity, is dependent on the distribution of stress in the soil from the applied preload, which is shown to be a function of soil-skirt interface roughness. Stresses are transferred to skirt tip level for the smooth skirted foundations leading to gains in shear strength being concentrated in the zone beneath tip level. Rough skirts carry a portion of the applied preload, with stresses transferred into the soil mass adjacent to the skirts leading to gains in strength laterally, adjacent to the rough foundation skirt.

- The consolidated undrained failure envelope may be determined by scaling the unconsolidated undrained envelope by the respective uniaxial consolidated undrained horizontal and moment capacities following full primary consolidation.

- The failure envelope following partial consolidation may be determined by scaling the fully consolidated undrained envelope by the partially consolidated values of uniaxial undrained horizontal and moment capacities.

Approximating expressions for uniaxial and combined capacities under pure vertical, horizontal and moment loading have been set out for prediction of consolidated undrained capacity for any degree of consolidation and relative preload for smooth and rough sided circular skirted foundations. The ability to scale the normalised unconsolidated undrained failure envelope to account for full or partial consolidation enables the results of this study to be synthesised into a relatively straightforward methodology for use in engineering practice.

The finite element results have shown that the majority of the gain in bearing capacity happens in the early stages of consolidation such that significant gains can be achieved in practical time frames. The results presented in this paper are valid for normally consolidated soil deposits that generate positive excess pore pressure during shearing – encompassing many soft, fine-grained deposits. The proposed methodology can be applied to other soil conditions provided that proper considerations are specifically accounted for the particular soil investigated.

This study has highlighted the potential conservatism in foundation design of using the in situ value of undrained shear strength of the soil in predictions of capacity. Foundations are often laid on the seabed for a period of time prior to operation during which the soil in the vicinity of the foundation will consolidate under the foundation self-weight, resulting in enhanced shear strength. Efficiencies in foundation size can be realised by taking into account the consolidation gain in undrained shear strength of the soil.

ACKNOWLEDGEMENTS

This work forms part of the activities of the Centre for Offshore Foundation Systems (COFS). Established in 1997 under the Australian Research Council's Special Research Centres Program. Supported as a node of the Australian Research Council's Centre of Excellence for Geotechnical Science and Engineering, and through the Fugro Chair in Geotechnics, the Lloyd's Register Foundation Chair and Centre of Excellence in Offshore Foundations and the Shell EMI Chair in Offshore Engineering. The second author is supported through ARC grant CE110001009. The work presented in this paper is supported through ARC grant DP140100684. This support is gratefully acknowledged.

NOTATION

A	Cross-sectional area of the base plate
c_{v0}	In-situ coefficient of consolidation
d	Skirt length

D	foundation diameter
e_0	In-situ void ratio
e_f	Final void ratio
f_σ	Stress factor
f_d	Depth factor
f_{su}	Strength factor
h	Normalized horizontal load (H/H_{uu})
h_{cu}	Normalized consolidated undrained pure horizontal capacity (H_{cu}/H_{uu})
$h_{cu,p}$	Normalized consolidated undrained pure horizontal capacity ($H_{cu,p}/H_{uu}$)
h_{max}	Normalized maximum allowable horizontal load (H_{max}/H_{uu})
H	Uniaxial (unconsolidated)horizontal load
H_{cu}	Consolidated undrained horizontal capacity following full primary
$H_{cu,p}$	Consolidated undrained horizontal capacity following partial consolidation
H_{uu}	Unconsolidated undrained horizontal capacity
k	Soil permeability
K_0	In-situ earth pressure coefficient of normally consolidated deposit
k_{su}	Shear strength gradient
m	Normalized moment (M/M_{uu})
m_{cu}	Normalized consolidated undrained pure moment capacity (M_{cu}/M_{uu})
$m_{cu,p}$	Normalized consolidated undrained pure moment capacity ($M_{cu,p}/M_{uu}$)
m_i, n_i	Fitting coefficients
M	Uniaxial (unconsolidated) moment
M_{cs}	Slope of the Critical State Line (CSL)
M_{cu}	Consolidated undrained moment capacity following full primary
$M_{cu,p}$	Consolidated undrained moment capacity following partial consolidation
M_{uu}	Unconsolidated undrained moment capacity
p'	Effective mean stress
p_0'	Initial effective mean stress
p_c'	Preconsolidation stress
q	Deviatoric stress
q_0	Initial effective deviatoric stress
q_f	Deviatoric stress at failure
R	Normally consolidated undrained strength ratio
RP	Reference point
s_u	Undrained shear strength

$s_{u,f}$	Final (post-consolidation) shear strength
$s_{u,i}$	Initial (pre-consolidation) shear strength
s_{um}	Undrained shear strength at mudline
t	Time
t_s	Skirt thickness
T	Non-dimensional time factor
T_{50}	Time for 50% consolidation to occur
$T_{50,g}$	Non-dimensional time required for 50% of the potential maximum uniaxial
$T_{50,s}$	Non-dimensional time factor for 50% consolidation settlement
v_p	Applied bearing pressure
V	Uniaxial (unconsolidated) vertical load
V_{cu}	Consolidated undrained vertical capacity following partial consolidation
$V_{cu,p}$	Consolidated undrained vertical capacity following full primary
V_p	Vertical preload
V_{uu}	Unconsolidated undrained vertical capacity
w_c	Consolidation settlement
α, β	Fitting coefficients
α_d, β_d	Depth factor fitting coefficients
α_{su}	Friction ratio of skirts
$\Delta p'_{pl}$	Operative increment in in plastic stress
Δu	Excess pore water pressure
Δu_i	Initial excess pore water pressure
φ'	Critical state friction angle
γ_w	Unit weight of water
κ	Slope of the recompression line
λ	Slope of the virgin compression line
κ_{su}	Soil heterogeneity index
σ'_v	In-situ vertical effective stress
σ'_h	In-situ horizontal effective stress
θ	Lode angle

REFERENCES

Butterfield, R., Houlsby, G.T. and Gottardi, G. (1997). Standardised sign conventions and notation for generally loaded foundations. *Géotechnique*, 47(4): 1051–1052.

Bransby, M.F. (2002). The undrained inclined load capacity of shallow foundations after consolidation under vertical loads. *Proc. 8th Numerical Models in Geomechanics (NUMOG)*, Rome, 431-437.

Britto, A.M. and Kusakabe, O. (1982). Stability of unsupported axisymmetric excavations in soft clay. *Géotechnique*, 32(2): 261-270.

Bye, A., Erbrich, C., Rognlien, B. and Tjelta, T.I. (1995). Geotechnical design of bucket foundations. *Proc. Annual Offshore Technology Conf.* Houston, Paper OTC 7793.

Byrne, B.W. and Houlsby, G.T., (2003). Foundations for offshore wind turbines. Philos Trans A Math Phys Eng Sci. Dec 15;361(1813):2909-30.

Chatterjee, S., Yan, Y., Randolph, M.F. and White, D.J. (2012). Elastoplastic consolidation beneath shallowly embedded offshore pipelines. *Géotechnique Letters* 2: 73-79.

Chatterjee, S., Gourvenec, S. and White, D.J. (2014) Assessment of the consolidated breakout response of partially embedded subsea pipelines. *Géotechnique*, 64(5): 391-399.

Chen, W. and Randolph, M.F. (2007). External radial stress changes and axial capacity for suction caissons in soft clay. *Géotechnique*, 57(6): 499-511.

Dassault Systèmes (2012). Abaqus analysis user's manual. Simulia Corp. Providence, RI, USA.

Feng, X. and Gourvenec, S. (2015) Consolidated undrained load-carrying capacity of mudmats under combined loading in six degrees-of-freedom. *Géotechnique*, 65(7): 563-575.

Fu, D., Gaudin, C., Tian, C., Bienen, B. and Cassidy, M.J. (2015). Effects of preloading with consolidation on undrained bearing capacity of skirted circular footings. *Géotechnique*, 65(3): 231-246.

Gourvenec, S. and Randolph, M.F. (2010) Consolidation beneath skirted foundations due to sustained loading. *International Journal of Geomechanics*, 10(1): 22 - 29.

Gourvenec, S.M., Vulpe, C. and Murthy, T.G. (2014). A method for predicting the consolidated undrained bearing capacity of shallow foundations. *Géotechnique*, 64(3): 215 – 225.

Gourvenec, S. and Barnett, S. (2011). Undrained failure envelope for skirted foundations under general loading. *Géotechnique*, 61(3): 263–270.

Jostad, H.P., Andersen, K.H. (2006). Potential benefits of using skirted foundations for jackup platforms. *Offshore Technology Conference (OTC)*, Houston, Texas, USA, OTC 18016.

Lehane, B.M. and Gaudin, C. (2005). Effects of drained pre-loading on the performance of shallow foundations on over consolidated clay. *Proc. Offshore Mechanics and Arctic Engineering* (OMAE), OMAE2005-67559.

Lehane, B.M. and Jardine, R.J. (2003). Effects of long-term preloading on the performance of a footing on clay. *Géotechnique*, 53(8): 689 - 695.

Mana, D.K.S, Gourvenec, S., Randolph, M.F. and Hossain, M.S. (2012) Failure mechanisms of skirted foundations in uplift and compression. *International Journal of Physical Modelling in Geotechnics*, 12(2): 47-62.

Mana, D.S.K., Gourvenec, S., Randolph, M.F. (2010). A numerical study of the vertical bearing capacity of skirted foundations. *Proc. 2nd International Symposium Frontiers in Offshore Geotechnics (ISFOG)*, Perth, Australia, 433-438.

Mana, D.K.S, Gourvenec, S. and Randolph, M.F. (2013). Experimental investigation of reverse end bearing of offshore shallow foundations. *Canadian Geotechnical Journal*, 50: 1022-1033.

Martin, C.M. (2003). New software for rigorous bearing capacity calculations. *Proc. British Geotech. Assoc. Int. Conf. on Foundations*, Dundee, 581-592.

Martin, C. M. and Randolph, M. F. (2001). Applications of the lower and upper bound theorems of plasticity to collapse of circular foundations. *Proc. 10th Int. Conf. Int. Assoc. of Computer Methods and Advances in Geomech (IACMAG), Tucson* **2**, 1417-1428.

Potts, D.M. and Zdravkovic, L. (1999). *Finite element analysis in geotechnical engineering – theory*. London, UK: Thomas Telford.

Randolph, M. F and Puzrin, A. M (2003). Upper bound limit analysis of circular foundations on clay under general loading. *Géotechnique*, 53(9): 785-796.

Roscoe, K.H. and Burland, J.B. (1968) On the4 generalised stress-strain behavior of "wet clay". *Engineering plasticity*. Cambridge University Press.

Stewart, D.P. (1992). *Lateral loading of pile bridge abutments due to embankment construction*. PhD thesis, University of Western Australia.

Supachawarote, C., Randolph, M.F. and Gourvenec, S. (2005). The effect of crack formation on the inclined pullout capacity of suction caissons. *Proceedings of the international Association of Computer Methods and Advances in Geomechanics Conference*, Turin, Italy: 19-24 June 2005, Balkema: 577-584.

Svano, G., Tjelta, T.I. (1996). Skirted spudcans – extending operational depth and improving performance. *Marine Structures*, 9(1): 129-148.

Vulpe, C. (2015) Design method for the undrained capacity of skirted circular foundations under combined loading: effect of deformable soil plug. *Géotechnique*, 65(8): 669-683.

Vulpe, C., Bienen, B. and Gaudin, C. (2013). Predicting the undrained capacity of skirted spudcans under combined loading. *Ocean Engineering*, 74, 178–188.

Vulpe, C. and Gourvenec, S. (2014) Effect of preloading on the response of a shallow skirted foundation. *Proceedings of the 33rd International Conference on Ocean, Offshore and Arctic Engineering*, San Francisco, USA, OMAE2014-23440.

Vulpe, C., Gourvenec, S., Leman, B. and Fung, K.N. (2016). A failure envelope approach for consolidated undrained capacity of shallow foundations. *Journal of Geotechnical and Geoenvironmental Engineering 14(4): 0401409 (DOI: 10.1061/(ASCE)GT.1943-5606.0001498)*

Vulpe, C., Gourvenec, S. and Power, M. (2014). A generalised failure envelope for undrained capacity of circular shallow foundations under general loading. *Géotechnique Letters*, 4: 187 – 196 (http://dx.doi.org/10.1680/geolett.14.00010).

Yun, G.I., Bransby, M.F. (2003). Centrifuge modelling of the horizontal capacity of skirted foundations on drained loose sand. *Proc. British Geotechnical Association International Conference on Foundations (ICOF)*, Dundee, UK, Thomas Telford.

Zdravkovic, L. Potts, D.M. and Jackson, C. (2003). Numerical study of the effect of preloading on undrained bearing capacity. *Int. J. Geomechanics* ASCE, September, 1 – 10.

LIST OF TABLES

LIST OF FIGURES

Figure 11. Normalised gain in undrained uniaxial vertical capacity after moment preloading and full primary consolidation for (a) rough interface and (b) smooth interface. Theoretical prediction using Equation 16 also shown.

Figure 12. Failure mechanisms under pure vertical, horizontal and moment loading following preloading and consolidation of skirted circular foundations with embedment ratio d/D = 0.5 for the discrete level of preload V_p/V_{uu} = 0.7

Figure 13. Stress paths at the centreline of the foundation (d/D = 0) during loading and consolidation: a) p’-q space; b) e-ln(p’) space

Figure 14. Normalised consolidated undrained uniaxial capacity after partial consolidation as a fraction of the normalised consolidated undrained uniaxial capacity after full primary consolidation for smooth skirted foundations.

Figure 15. Failure envelopes as function of relative preload: a) & b) unconsolidated undrained c) & d) consolidated undrained

Figure 16. Normalised consolidated undrained envelope after full primary consolidation under varying preload levels compared to curve fits for; a), c), rough interface; and b), d) smooth interface.

Figure 17. Normalised consolidated undrained envelope after partial consolidation under varying preload levels compared to curve fits for; a), c) rough interface; and b), d) smooth interface.

TABLES

Table 1. Soil properties used in finite element analyses

Parameter input for FE analyses	Magnitude
Index and engineering parameters	
Saturated Bulk Unit Weight (kN/m^3)	17.18
Permeability (m/s)	$1.3\ 10^{-10}$
Elastic parameters (as a porous elastic material)	
Recompression Index (κ)	0.044
Poisson's Ratio (ν')	0.25
Elastic shear modulus (G)	$50p'_0$
Tensile Limit	0
Clay plasticity parameters	
Virgin compression Index (λ)	0.205
Stress Ratio at Critical State (M_{cs})	0.89
Wet Yield Surface Size*	1
Flow Stress Ratio**	1
Intercept (e_1, at p'=1 kPa on CSL)	2.14

*The wet yield surface size is a parameter defining the size of the yield surface on the "wet" side of critical state, β. (β = 1 means that the yield surface is a symmetric ellipse).
**The flow stress ratio represents the ratio of flow stress in triaxial tension to the flow stress in triaxial compression

Table 2. Definition of notation

	Vertical	**Horizontal**	**Rotational**
Load	V_p (preload)	H	M
Uniaxial (unconsolidated) undrained capacity	V_{uu}	H_{uu}	M_{uu}
Normalized load	$v_p = V_p/V_{uu}$	$h = H/H_{uu}$	$m = M/M_{uu}$
Consolidated undrained pure uniaxial capacity	V_{cu}	H_{cu}	M_{cu}
Normalized consolidated undrained pure uniaxial capacity	$v_{cu} = V_{cu} / V_{uu}$	$h_{cu} = H_{cu} / H_{uu}$	$m_{cu} = M_{cu} / M_{uu}$

Table 3. Stress and strength factor $f_\sigma f_{su}$ for surface circular foundations for critical state interpretation

Loading direction	$f_\sigma f_{su}$
V	0.43
H	0.88
M	0.57

Table 4. Coefficients α_d and β_d for defining the depth scaling factor f_d for critical state interpretation, Eqn 17

Soil-skirt interface roughness	Loading direction	$\alpha_{d,1}$	$\alpha_{d,2}$	$\beta_{d,1}$	$\beta_{d,2}$
rough	**V**	-1.32	1.1	1.34	-0.44
	H	-2.77	2.99	0.73	-0.38
	M	0.4	-1.79	1.42	-1.18
smooth	**V**	-0.71	0.53	1.56	-2.23
	H	-3.11	3.75	0.12	0.04
	M	1.17	-3.12	0.43	0.21

Table 5. Non-dimensional time factor for 50% partial consolidation settlement, $T_{50,s}$

d/D	rough interface	smooth interface
0.1	0.28	0.28
0.25	0.34	0.32
0.5	0.4	0.35

Table 6. Fitting coefficient m_i, where i = V, H, or M, for determining the gain in capacity following partial consolidation for rough and smooth skirted circular foundations

m_V	0.8
m_H	1.2
m_M	1.2

Table 7. Fitting parameters for approximating expression for unconsolidated undrained failure envelope for skirted circular foundations with rough soil-skirt interface.

	α				β			
	d/D							
κ_{su}	**0**	**0.1**	**0.25**	**0.5**	**0**	**0.1**	**0.25**	**0.5**
0	1.63	1.89	2.10	1.83	-0.05	-0.16	-0.44	-0.66
6	2.00	1.70	2.15	1.96	0.06	0.08	-0.22	-0.53
20	2.46	1.66	2.10	2.04	-0.01	0.27	-0.11	-0.49
60	2.89	1.75	2.10	2.03	0.13	0.40	-0.07	-0.46
100	3.12	1.76	2.11	2.03	0.13	0.44	-0.07	-0.46

Table 8. Fitting parameters for approximating expression for unconsolidated undrained failure envelope for skirted circular foundations with smooth soil-skirt interface.

	α				β			
	d/D							
κ_{su}	**0**	**0.1**	**0.25**	**0.5**	**0**	**0.1**	**0.25**	**0.5**
0	1.63	1.94	1.97	1.73	-0.05	-0.01	-0.26	-0.58
6	2.00	1.65	2.11	1.76	0.06	0.26	0.01	-0.42
20	2.46	1.66	2.16	1.94	-0.01	0.40	0.13	-0.33
60	2.89	1.76	2.11	1.93	0.13	0.53	0.20	-0.30
100	3.12	1.82	2.29	1.94	0.13	0.56	0.18	-0.30

Table 9. Values of h_{max}/h^*_{uu} for vertical load mobilisation $0 \leq V_p/V_{uu} \leq 1$ for skirted circular foundations with rough and smooth soil-skirt interface roughness

	rough soil-skirt interface					smooth soil-skirt interface				
	κ_{su}					κ_{su}				
d/D	**0**	**6**	**20**	**60**	**100**	**0**	**6**	**20**	**60**	**100**
0	1	1	1	1	1	1	1	1	1	1
0.1	1	1	1	-1.07	-1.1	1	1	-1.09	-1.19	-1.22
0.25	1.11	1.03	1.01	1	1	1.02	1	1	1	1
0.5	1.37	1.17	1.15	1.13	1.12	1.17	1.03	1.01	1.01	1.01

Table 10. Summary of proposed procedure.

	Activity	**Reference**
Step 1	Calculate uniaxial unconsolidated undrained capacities, V_{uu}, H_{uu} and M_{uu} for particular foundation geometry and shear strength soil profile.	Vulpe, 2015
Step 2	Calculate normalised preload $v_p = V_p/V_{uu}$.	
Step 3	Calculate the normalised consolidated undrained pure uniaxial capacities v_{cu}, h_{cu} and m_{cu} for the particular foundation geometry, relative preload and interface roughness.	Equations **13 - 17** and Table 3 and Table 4
Step 4	Calculate the normalised loads h and m for the selected foundation geometry and desired H and M loads.	
Step 5	Calculate the normalised loads h^* and m^* for the selected foundation geometry and level of vertical preload V_p/V_{uu}.	Equation **21**
Step 6	Plot normalised unconsolidated undrained VHM failure envelope from approximating expression in h/h^* and m/m^* space for the desired V_p/V_{uu}, d/D, soil heterogeneity and soil-skirt interface roughness.	Vulpe, 2015
Step 7	Plot the VHM failure envelope for the fully consolidated undrained condition by scaling the normalised undrained unconsolidated curve by the normalised consolidated uniaxial capacities, h_{cu} and m_{cu}, determined in Step 3.	
Step 8	Calculate $h_{cu,p}$ and $m_{cu,p}$ for the desired consolidation time and for the particular foundation geometry and interface roughness. Scale the fully consolidated failure envelope (from Step 7) by $h_{cu,p}/h_{cu}$ and $m_{cu,p}/m_{cu}$ factors.	Equations **18** and **19** and Table 5 and Table 6

FIGURES

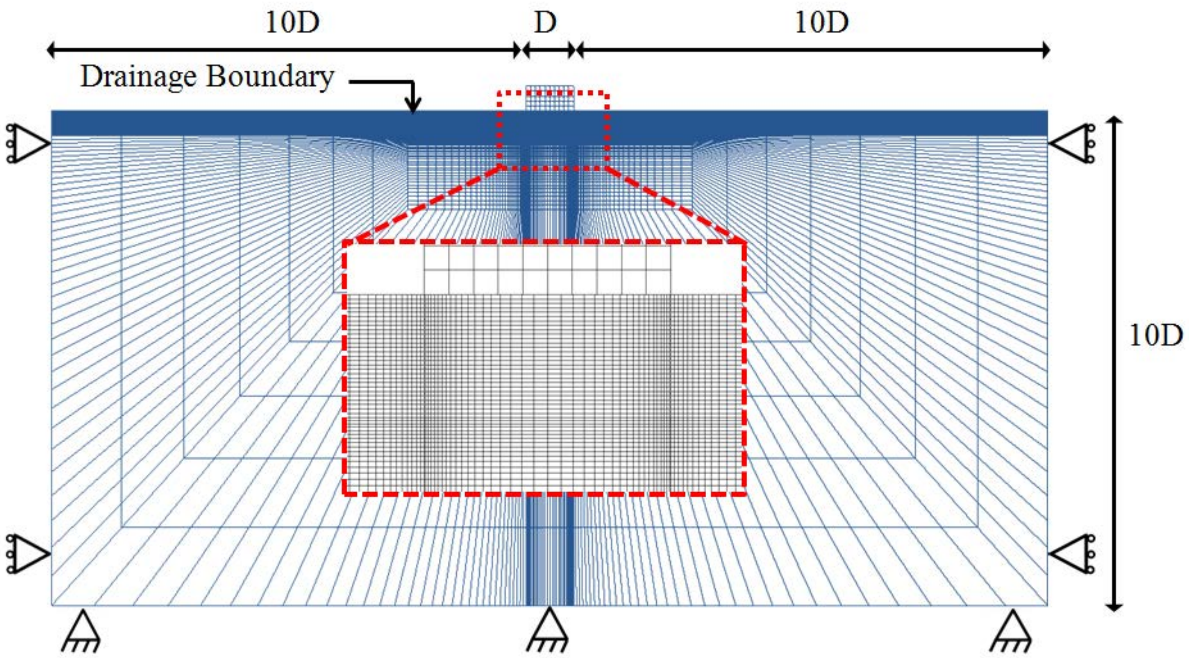

Figure 1. Example of finite element mesh (d/D = 0.50)

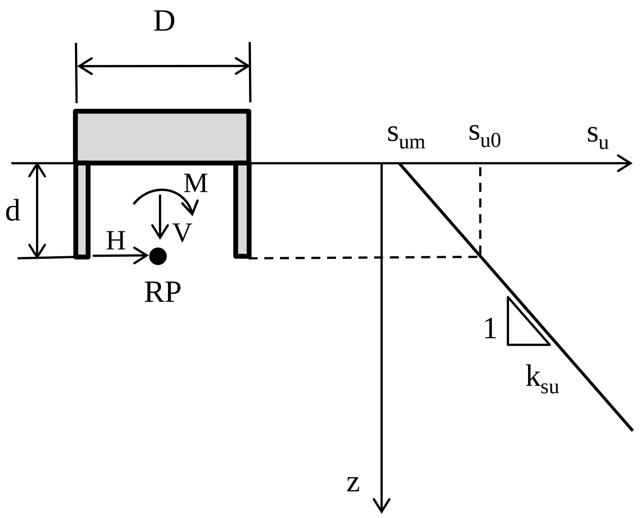

Figure 2. Foundation geometry, reference point and soil shear strength profile

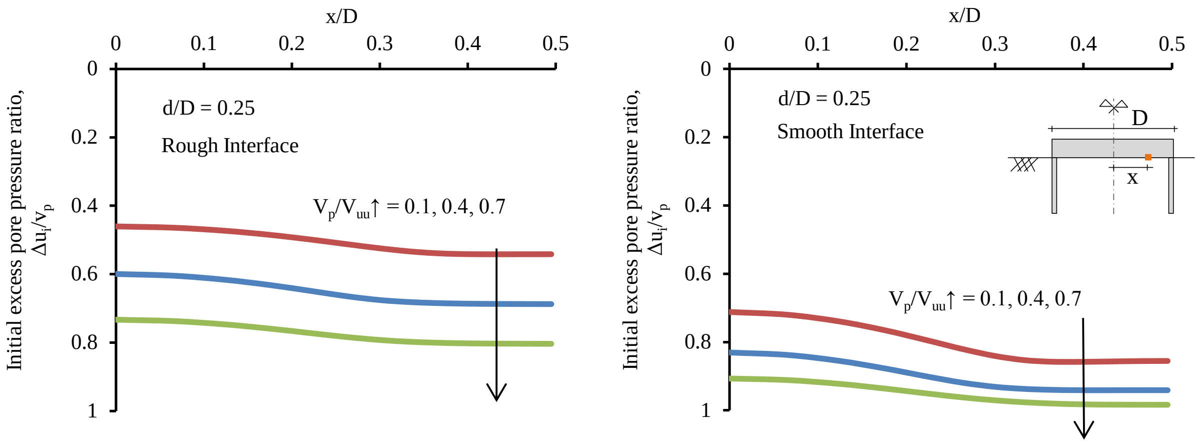

Figure 3. Effect of embedment on the initial excess pore pressure distribution beneath the base plate

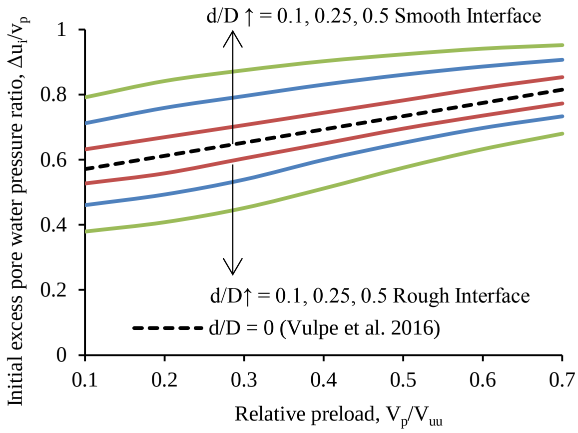

Figure 4. Effect of embedment on the initial excess pore pressure ratio underneath the base plate at the centreline

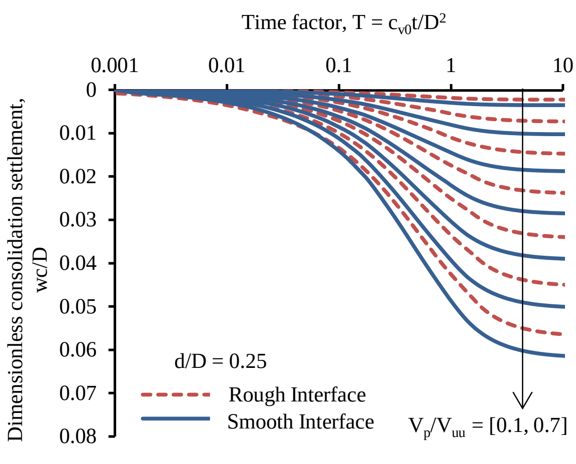

Figure 5. Effect of preload and interface roughness on the foundation time-settlement response, example shown for d/D = 0.25

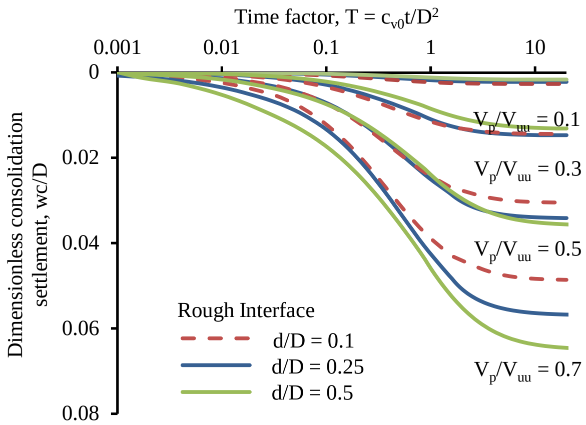

Figure 6. Effect of embedment ratio on foundation time-settlement response at the centreline of skirted circular foundations with rough soil-skirt interface

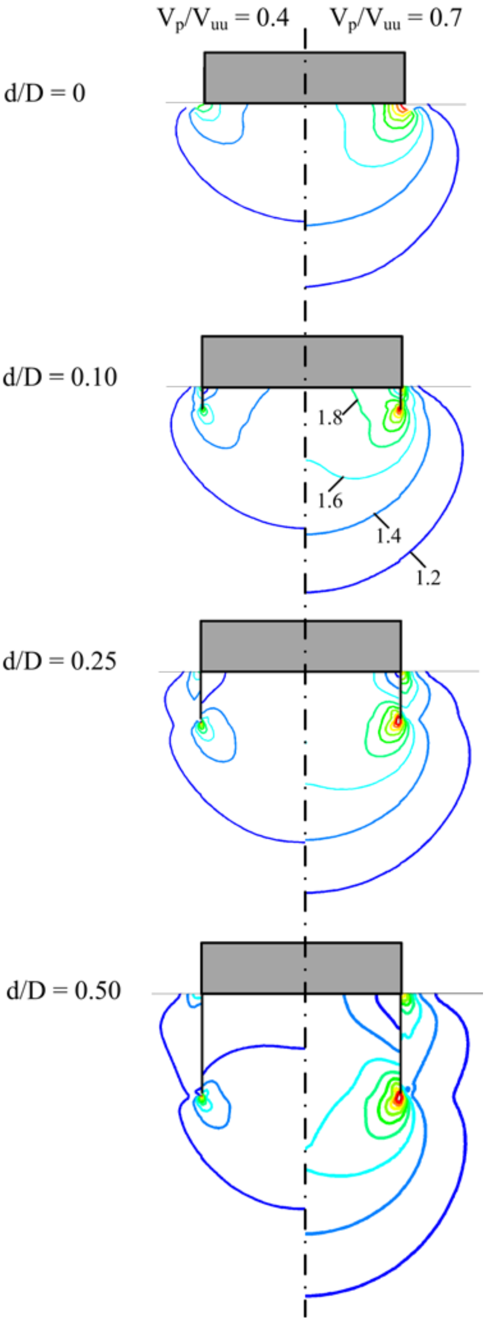

Figure 7. Effect of relative preload on gains in undrained shear strength after full primary consolidation, example for foundations with rough interface. Contours of final to in situ undrained strength, $s_{u,f}/s_{u,i}$ = 1.2, 1.4 etc

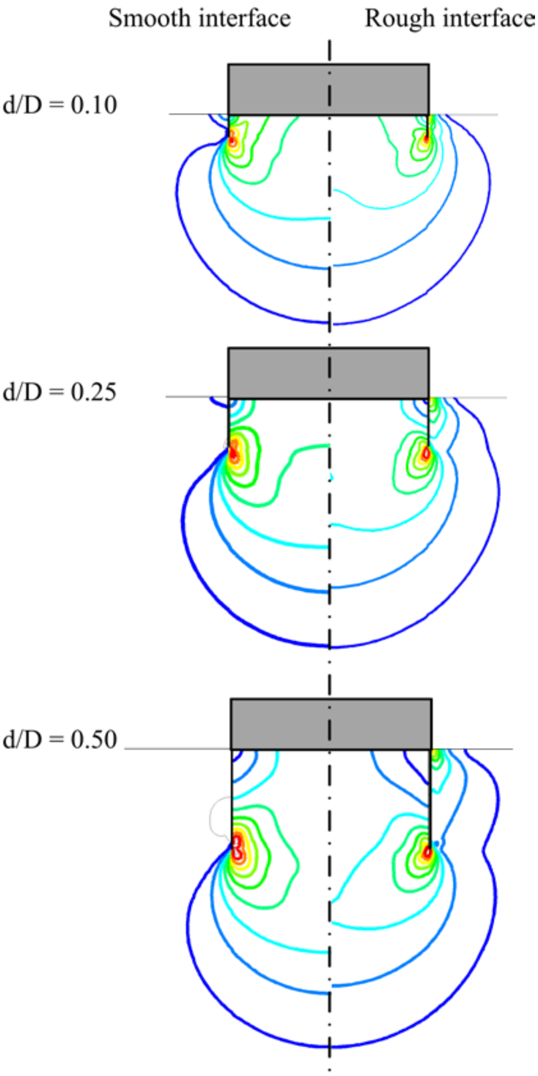

Figure 8. Effect of soil-skirt interface roughness on gains in undrained shear strength after full primary consolidation, examples for relative preload V_p/V_{uu} = 0.7.

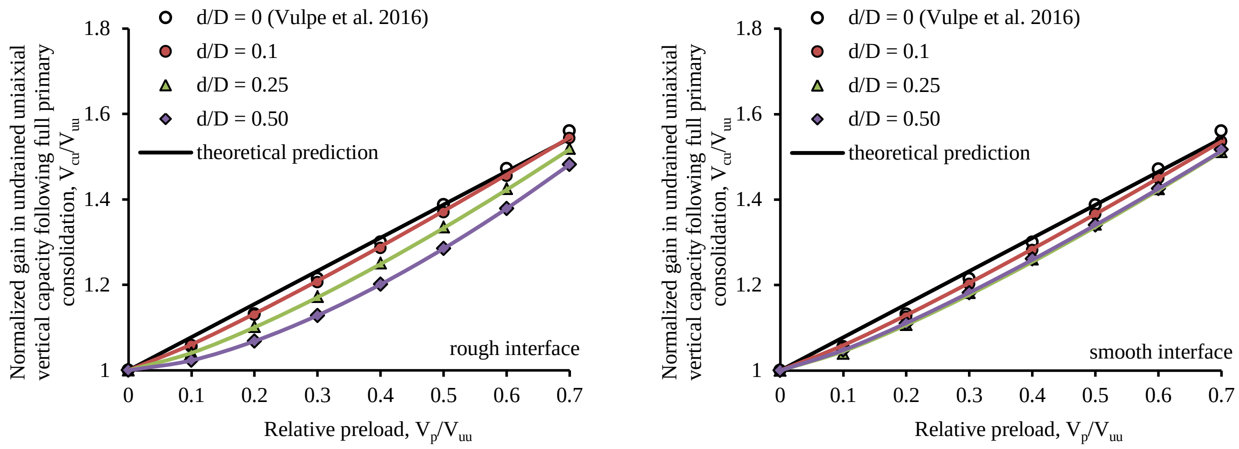

a) b)

Figure 9. Normalised gain in undrained uniaxial vertical capacity after vertical preloading and full primary consolidation for (a) rough interface and (b) smooth interface. Theoretical prediction using Equation 16 also shown.

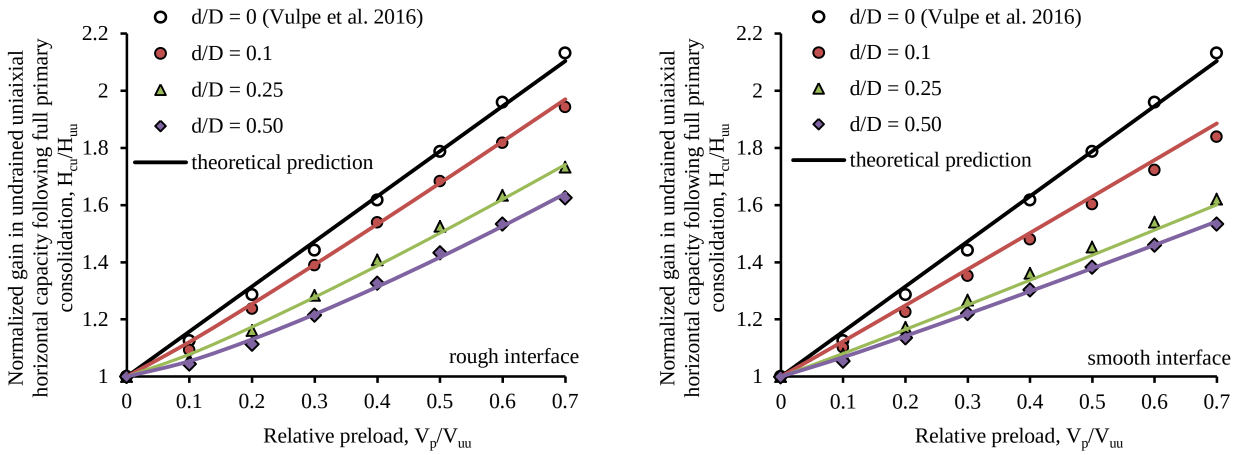

a) b)

Figure 10. Normalised gain in undrained uniaxial horizontal capacity after vertical preloading and full primary consolidation for (a) rough interface and (b) smooth interface. Theoretical prediction using Equation 16 also shown.

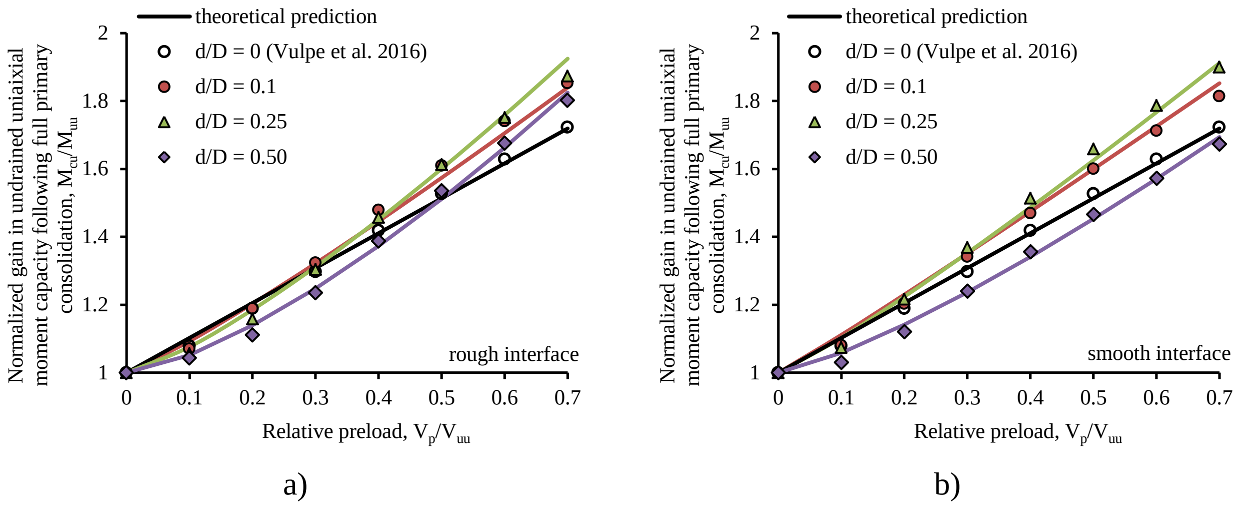

Figure 11. **Normalised gain in undrained uniaxial vertical capacity after moment preloading and full primary consolidation for (a) rough interface and (b) smooth interface. Theoretical prediction using Equation 16 also shown.**

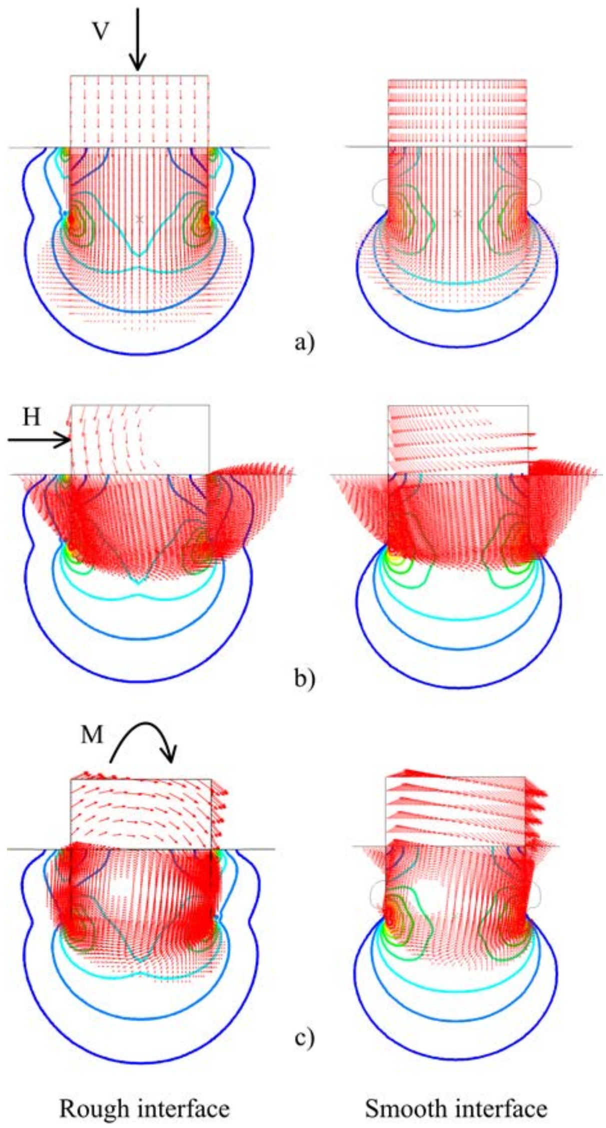

Figure 12. Failure mechanisms under pure vertical, horizontal and moment loading following preloading and consolidation of skirted circular foundations with embedment ratio d/D = 0.5 for the discrete level of preload V_p/V_{uu} = 0.7

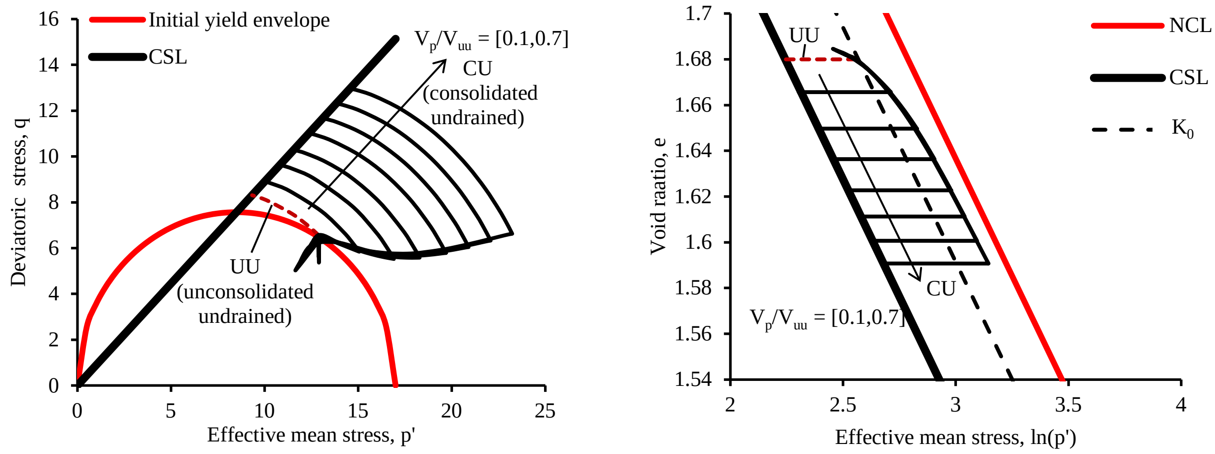

Figure 13. Stress paths at the centreline of the foundation (d/D = 0) during loading and consolidation: a) p'-q space; b) e-ln(p') space

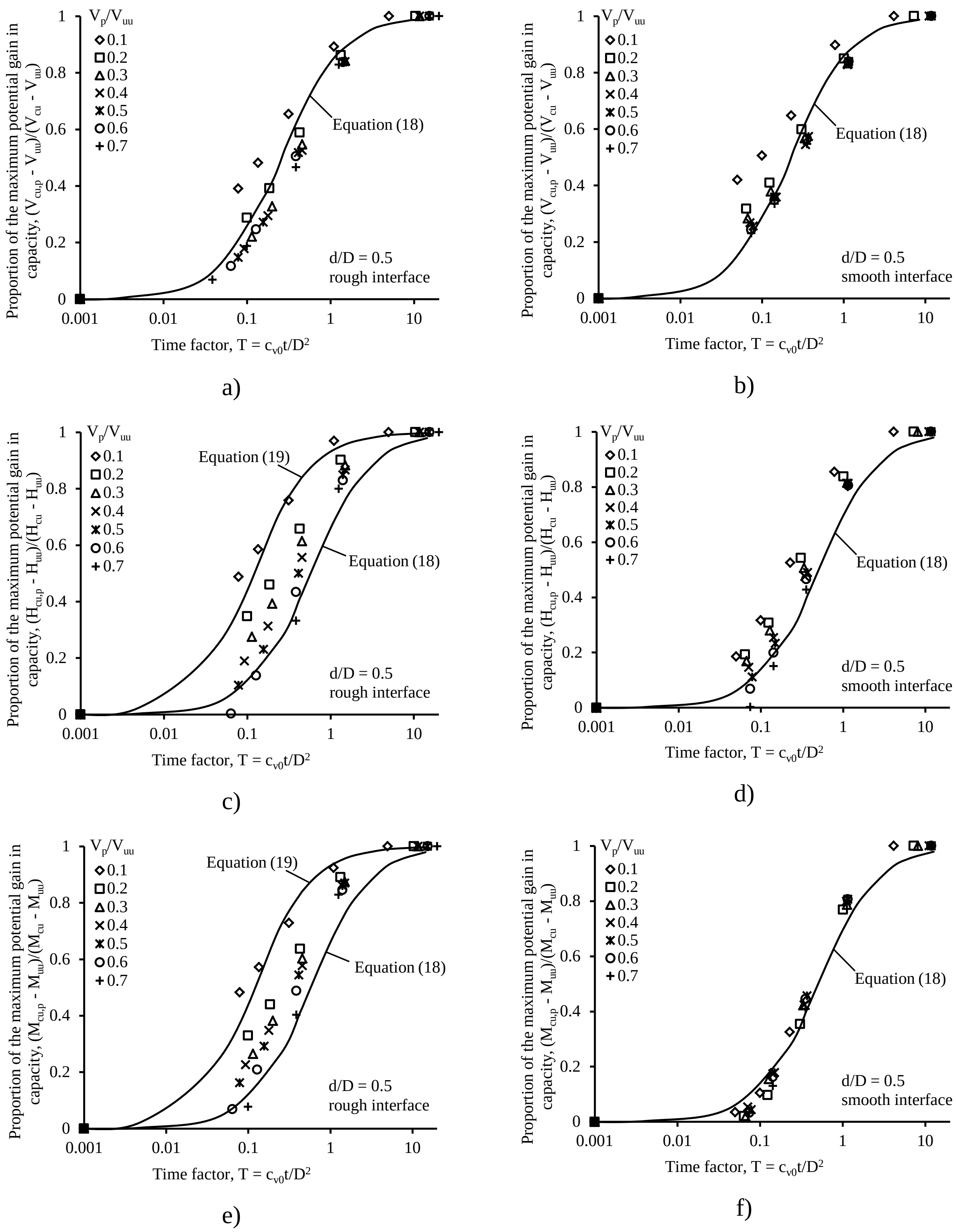

Figure 14. Normalised consolidated undrained uniaxial capacity after partial consolidation as a fraction of the normalised consolidated undrained uniaxial capacity after full primary consolidation for smooth skirted foundations.

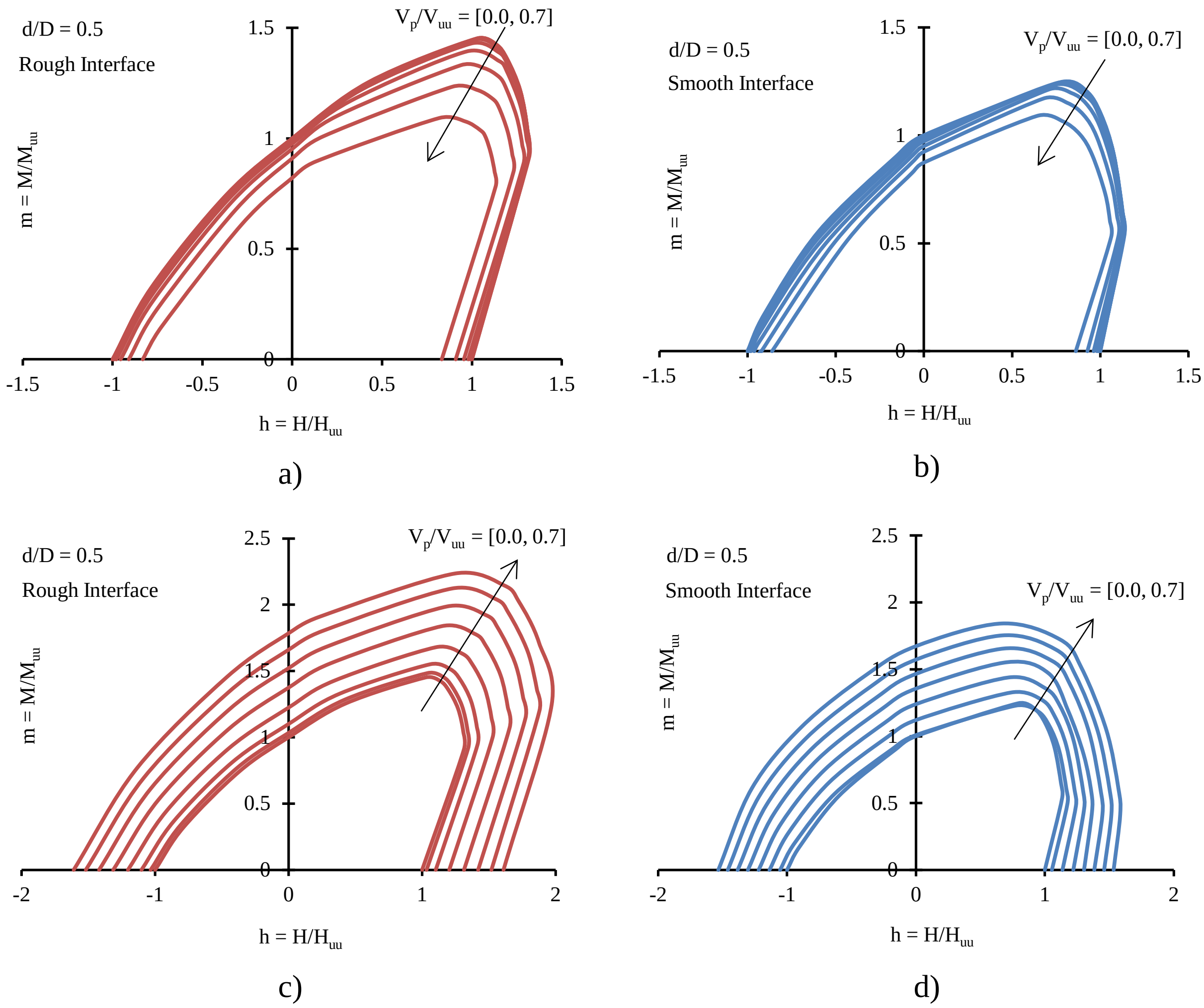

Figure 15. Failure envelopes as function of relative preload: a) & b) unconsolidated undrained c) & d) consolidated undrained

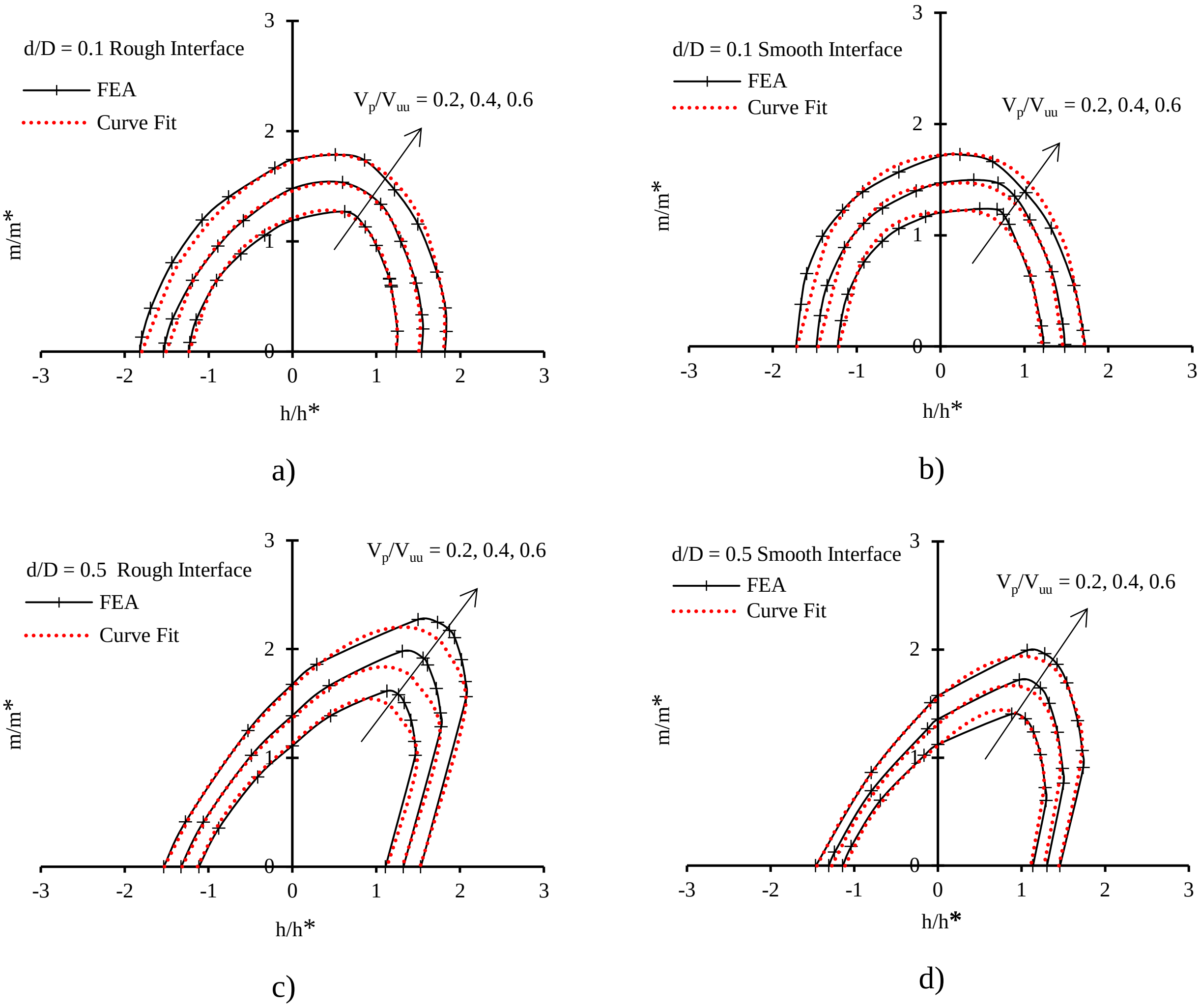

Figure 16. Normalised consolidated undrained envelope after full primary consolidation under varying preload levels compared to curve fits for; a), c), rough interface; and b), d) smooth interface.

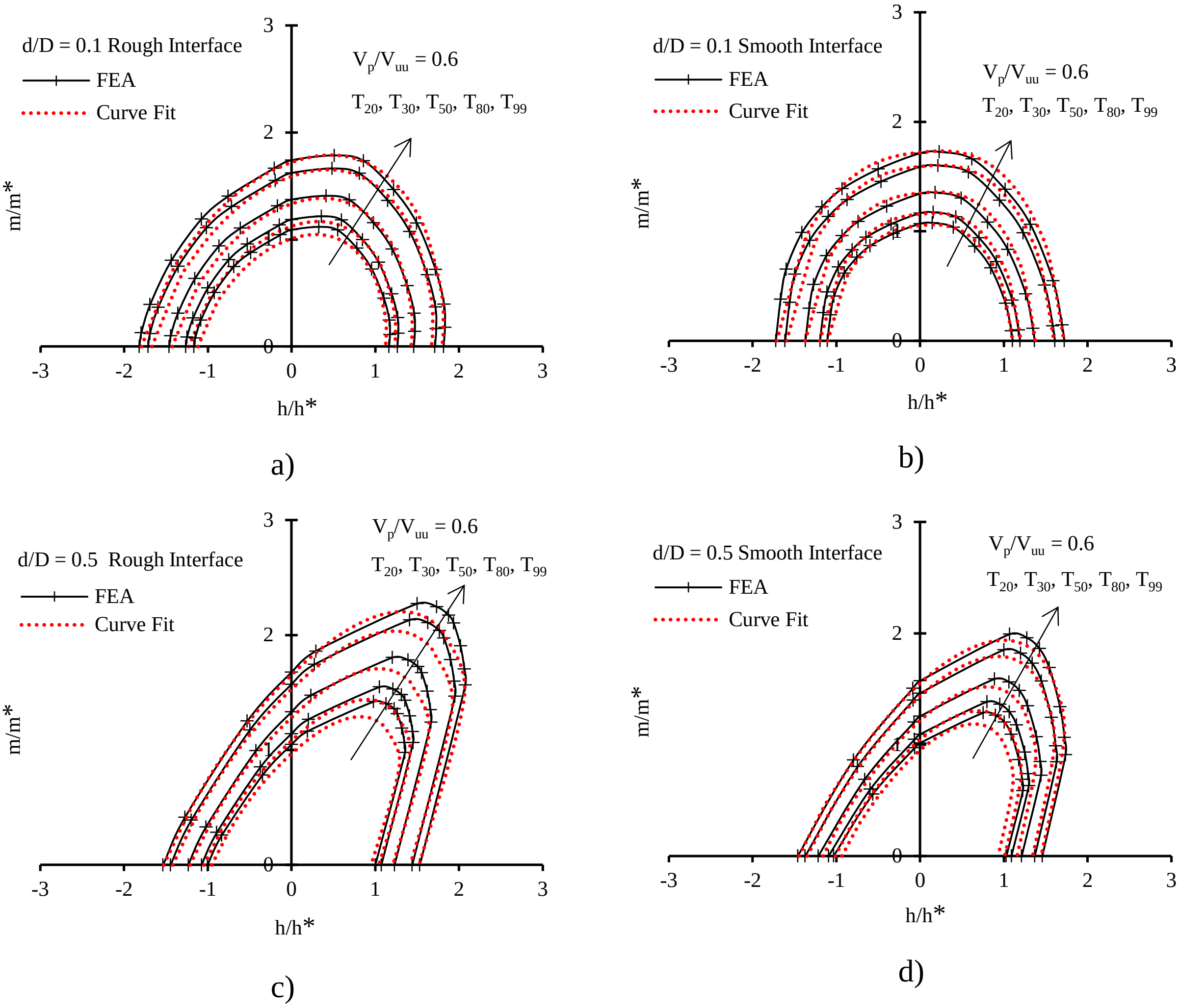

Figure 17. Normalised consolidated undrained envelope after partial consolidation under varying preload levels compared to curve fits for; a), c) rough interface; and b), d) smooth interface.